

1 **Slow-paced inspiration regularizes alpha phase dynamics in the**  
2 **human brain**

3  
4 ***Shen-Mou Hsu<sup>1</sup>, Chih-Hsin Tseng<sup>2</sup>, Chao-Hsien Hsieh<sup>1,3</sup>, Chang-Wei Hsieh<sup>4</sup>***

5  
6  
7 <sup>1</sup> Imaging Center for Integrated Body, Mind and Culture Research, National Taiwan  
8 University, Taipei, Taiwan (R.O.C.)

9 <sup>2</sup> Graduate Institute of Biomedical Electronic and Bioinformatics, National Taiwan  
10 University, Taipei, Taiwan (R.O.C.)

11 <sup>3</sup> Interdisciplinary MRI/MRS Laboratory, Department of Electrical Engineering,  
12 National Taiwan University, Taipei, Taiwan (R.O.C.)

13 <sup>4</sup> Department of Photonic and Communication Engineering, Asia University, Taichung,  
14 Taiwan (R.O.C.)

15  
16  
17 *Corresponding author:*

18  
19 Shen-Mou Hsu  
20 Imaging Center for Integrated Body, Mind and Culture Research  
21 National Taiwan University  
22 No.49, Fanglan Rd., Da'an Dist.  
23 Taipei, 10617  
24 Taiwan (R.O.C.)  
25 Tel: 886-2-27326243  
26 Email: smhsu@ntu.edu.tw

27

28 **Abstract**

29 The phase of low-frequency, rhythmic cortical activity is essential for organizing  
30 brain processes because it provides a recurrent temporal frame for information coding.  
31 However, the low-frequency cortical phase exhibits great flexibility in response to  
32 external influences. Given that brain rhythms have been found to track respiratory  
33 inputs, we hypothesized that slow breathing, commonly associated with mental  
34 regulation, could reorganize the relationship between these two rhythmic systems  
35 through the adjustment of the cortical phase to such a slow train of inputs. Based on  
36 simultaneous magnetoencephalography and respiratory measurements, we report that  
37 while participants performed paced breathing, slow relative to normal breathing  
38 modulated cortical phase activity in the alpha range across widespread brain areas.  
39 Such modulation effects were specifically locked to the middle of the inspiration stage  
40 and exhibited a well-structured pattern. At the single-subject level, the phase angles  
41 underlying the effects became more likely to be diametrically opposed across breaths,  
42 indicating unique and consistent phase adjustment to slow inspiratory inputs. Neither  
43 cardiac fluctuations nor breathing-unrelated task effects could account for the findings.  
44 We suggest that slow-paced inspiration could organize the cortical phase in a  
45 regularized phase pattern, revealing a rhythmic but dynamic neural network integrated  
46 with different neurophysiological systems through volitional control.

47

48 **Keywords:** breathing; MEG; oscillation; phase; alpha

49

50 **Significance Statement**

51 Breathing is more complicated than a simple gas exchange, as it is integrated with  
52 numerous cognitive and emotional functions. Controlled slow breathing has often  
53 been used to regulate mental processes. This magnetoencephalography study  
54 demonstrates that slow-paced relative to normal-paced inspiration could organize the  
55 timing of alpha rhythmic activities across breathing cycles in a structured manner over  
56 widespread brain areas. Our results reveal how a volitionally controlled change in  
57 respiratory behavior could systematically modulate cortical activity.

58

59 **Introduction**

60 The phase of rhythmic cortical activity, particularly in the theta (4-8 Hz) and alpha  
61 (8-14 Hz) ranges, is central to organizing brain processes (Sauseng and Klimesch  
62 2008; Schroeder and Lakatos 2009; Thut et al. 2012; vanRullen 2016; Varela et al.  
63 2001). The gating of neural transmission may be mediated by phase (Schroeder and  
64 Lakatos 2009; vanRullen 2016). In this view, cyclic phases reflect the fluctuations of  
65 cortical excitability such that events that coincide with the phases indexing high  
66 excitability are amplified and vice versa. Phase is also involved in mediating neural  
67 communication such that communication is facilitated when the phases of two  
68 neuronal assemblies are in synchrony (Sauseng and Klimesch 2008; Varela et al.  
69 2001). All of these functions are construed as reflecting the common principle that  
70 rhythmic phases act as a temporal frame for information coding. One of the key  
71 features of such phase coding is its flexible dynamics. Accumulating evidence has  
72 shown that rhythmic phase activity can be adjusted according to bottom-up,  
73 stimulus-driven inputs (Luo and Poeppel 2007; Spaak et al. 2014) or top-down,  
74 expectation- or attention-related inputs (Lakatos et al. 2008; Stefanics et al. 2010). In  
75 general, these phenomena are manifested in terms of phase adjustment, as indexed by  
76 consistent, event-related phase clustering towards a certain direction, in response to a  
77 train of extrinsic and intrinsic inputs (Sauseng and Klimesch 2008; Thut et al. 2012;  
78 Voloh and Womelsdorf 2016).

79 Although the interaction between the brain and the physiological systems has been  
80 documented (Critchley and Garfinkel 2018; Varga and Heck 2017), it remains unclear

## The effect of respiration on the brain

81 whether and how bodily inputs contribute to the shaping of cortical phase dynamics.  
82 Breathing is one of the vital rhythms of human life and constitutes one possible source  
83 that may influence ongoing, low-frequency phase dynamics. First, breathing may  
84 create rhythmic inputs to the human brain directly either via the mechanical or  
85 thermal sensation of airflow through the nasal cavity or via interoceptive signals from  
86 the respiratory system through the brainstem (Del Negro et al. 2018; Heck et al. 2017;  
87 Lorig 2007). In addition, although breathing occurs effortlessly and without thought,  
88 it is exquisitely coordinated with a multitude of cognitive and emotional functions  
89 (Arsenault et al. 2013; Flexman et al. 1974; Perl et al. 2019; Zelano et al. 2016).  
90 Furthermore, recent animal and human studies have reported that natural breathing  
91 can drive rhythmic brain activity across multiple brain areas, prominently in the  
92 olfactory cortex, the frontal cortex and the subcortical structure (Herrero et al. 2018;  
93 Ito et al. 2014; Tort et al. 2018; Zelano et al. 2016).

94 Notably, the pace of breathing is not fixed. In particular, slow breathing has been  
95 associated with mental calmness and is therefore thought to provide a health benefit  
96 (Boiten et al. 1994; Homma and Masaoka 2008; Kreibig 2010). Indeed, because  
97 breathing can be partly brought under voluntary control, conscious pacing of  
98 breathing at a slow rate is often embraced by meditative techniques to regulate  
99 cognitive and emotional states (Lutz et al. 2004; Paul et al. 2013; Zeidan et al. 2010).  
100 Therefore, given that brain and respiratory rhythms are highly correlated, we  
101 hypothesized that a slow breathing pace could reorganize the relationship between  
102 these two rhythmic systems. The process might be manifested as an adjustment of the

103 low-frequency cortical phase to such a slow train of respiratory inputs. Through  
104 simultaneous respiration and magnetoencephalography (MEG) measurements, the  
105 current study tested our hypothesis by instructing participants to breathe at a slow  
106 (0.125 Hz, below the normal range: 0.2 – 0.3 Hz (Barrett et al. 2010)) or a normal  
107 pace (0.25 Hz, within the normal range). By systematically manipulating the interplay  
108 between the brain and respiratory systems in a controlled manner, we investigated  
109 whether different breathing paces led to differential phase adjustment.

110

## 111 **Materials and Methods**

112 **Participants.** Fifteen right-handed participants without previous neurological or  
113 psychiatric history were enrolled in this study (12 males and 3 females, mean age  $\pm$   
114  $SD = 26.27 \pm 3.22$  years, range = 22 – 32). All participants had normal or  
115 corrected-to-normal vision and provided written informed consent. All procedures  
116 were approved by the ethics committee of National Taiwan University. Because no  
117 prior similar study had been conducted, this number of participants was determined  
118 on the basis of previous parallel research on mind-body interaction (Critchley and  
119 Garfinkel 2018). Despite this, the effect size of the group-level result was large  
120 (Cohen's  $d$  for each point within the significant cluster: mean  $\pm$   $SD = 1.03 \pm 0.25$ ,  
121 range = 0.43 – 2.17), and the subsequent single-subject significant findings during  
122 slow breathing were consistently observed for every participant. Accordingly, we  
123 suggest that the robustness of the results can be justified.

124

## The effect of respiration on the brain

125 **Task.** Participants performed paced breathing by following the cues (“|” or “ - ”) at  
126 the center of the screen, which indicated the onset of expiration or inspiration. The  
127 alternation rate between the two cues was 2 s or 4 s, resulting in a regular breathing  
128 rate of 0.25 (4 s/ breath) or 0.125 Hz (8 s/ breath) in the normal- and slow-breathing  
129 conditions, respectively. Each condition consisted of two runs, and each run lasted 5  
130 min, with an approximately 1-min break between the runs. The cue types and the  
131 orders of the conditions were randomized across participants. Before each experiment,  
132 participants were acquainted with the procedure with a practice session and instructed  
133 to breathe through their noses because evidence has noted the importance of nasal  
134 breathing on cortical activity (Zelano et al. 2016). Their breathing conditions were  
135 monitored through a video camera located inside a magnetically shielded room.

136

137 **Data recordings.** MEG recordings were performed using a 306-channel whole-head  
138 MEG system (Elekta Neuromag TRIUX) with a sampling rate of 1000 Hz. Several  
139 physiological signals were simultaneously acquired. Eye-related activities were  
140 monitored via vertical and horizontal electrooculography (EOG). Electrocardiography  
141 (ECG) electrodes were placed over the chest close to the left and right clavicles.  
142 Respiratory activity was obtained via a respiratory belt positioned around the chest at  
143 the level of the armpits (respiratory transducer TSD201 BIOPAC system) and  
144 low-pass filtered (10 Hz) online. These signals were connected to and synchronized  
145 via the MEG acquisition system. All recorded data were subsequently analyzed using  
146 the FieldTrip toolbox (Oostenveld et al. 2011) in combination with MATLAB

The effect of respiration on the brain

147 (MathWorks) and R software (<http://www.R-project.org>). The data that support the  
148 findings of this study are available on request from the corresponding author.

149

150 **Head movement.** To ensure that the distinct patterns of chest movements between the  
151 inspiratory and respiratory phases did not propagate to the head and in turn bias the  
152 results, we continuously monitored the participants' head positions relative to the  
153 MEG sensors using a set of head localization coils placed at the nasion and the left  
154 and right ear canals. The results of the head movements, including the displacements  
155 and rotation angles of head positions along the x, y or z axes, were estimated using the  
156 Maxfilter software (Elekta Neuromag). Because the sampling resolution (1 Hz) of the  
157 continuous head positions was limited, the results of each head position parameter  
158 were averaged across the entire expiratory or inspiratory period. For every  
159 head-motion parameter, no significant difference was found between the inspiratory  
160 and expiratory periods in each condition or between the slow-breathing and  
161 normal-breathing conditions in each period (two-tailed paired t-test, all  $t(14)s \leq 1.86$ ,  
162 all  $ps \geq 0.09$ ).

163

164 **Data preprocessing.** The first 30 s of the data were discarded from the analysis to  
165 ensure steady breathing. Breathing cycles were estimated by detecting the intervals  
166 between two peaks of inspiration (i.e., one breath). Continuous MEG data were  
167 segmented according to the breathing cycles but extended from 1 s before to 1 s after  
168 the cycle period to avoid edge effects during spectral analysis. Trials contaminated



## The effect of respiration on the brain

169 with muscular artifacts were visually identified and rejected. Eye movements, eye  
170 blinks, and cardiac artifacts were removed using independent component analysis  
171 implemented in the FieldTrip toolbox (3-4 components removed). To minimize the  
172 contributions of signal noise, we considered only the trials with durations less than  
173 0.75 SD from the median. To ensure that participants followed the cues indicating  
174 inhalation and exhalation, we imposed an additional constraint by excluding the trials  
175 in which the mean inspiration and expiration onsets were more than 2 SD from the  
176 cues.

177

178 **Respiratory and ECG analysis.** To characterize breathing rates, we performed a fast  
179 Fourier transform analysis to calculate the power spectrum of the continuous  
180 respiratory signals. The dominant breathing frequency, as manifested by peak power,  
181 was determined in each participant. To ensure that the participants breathed in a  
182 normal manner without holding their breath during the slow-breathing condition, we  
183 computed the first derivative of the respiratory signal. If the breath was held, the  
184 respiratory signal fluctuated around a horizontal line, yielding multiple zero crossings  
185 in the curve derived from the calculated first derivative. However, for individual trials  
186 and participants, only three zero crossings were observed that were derived from two  
187 peaks of inspiration and one peak of expiration, indicating that participants did not  
188 significantly change their breathing behavior because of the slow pace. Heartbeat data  
189 (QRS complex) were extracted from the ECGs utilizing the Pan-Tompkins detection

The effect of respiration on the brain

190 algorithm (Pan and Tompkins 1985). Two participants were removed from the ECG  
191 analysis due to excessive noisy signals.

192

193 **Time-frequency representations of respiration-locked MEG data.** The  
194 instantaneous amplitude and phase at each sensor-time-frequency point were  
195 extracted using the Hilbert transform. Before the transform, the data were bandpass  
196 filtered (finite impulse response (FIR) filter, filter order dependent upon frequency  
197 band and data length (default setting in FieldTrip)) to create 13 frequency steps, with  
198 center frequencies from 2 to 14 Hz and bandwidths of 1 Hz.

199

200 **Unity-based time normalization of respiration-locked MEG data.** Given varying  
201 lengths of respiration-locked MEG trials within each condition and between  
202 conditions, we remapped the time course of each trial onto a common time scale that  
203 described the course of a breathing cycle to facilitate the subsequent phase-coherence  
204 computation and between-condition comparison. Unity-based time normalization was  
205 performed for the corresponding expiratory or inspiratory period of every trial within  
206 individual participants and conditions:

$$T_{normalized}(n, s, f) = \frac{T(n, s, f) - T_{EX/IN}^{onset}(n, s, f)}{T_{EX/IN}^{offset}(n, s, f) - T_{EX/IN}^{onset}(n, s, f)},$$

207 where  $T_{normalized}$  denotes a given normalized time point for each trial  $n$ , sensor  $s$ ,  
208 and frequency  $f$ .  $T$ ,  $T_{EX/IN}^{onset}$ , and  $T_{EX/IN}^{offset}$  denote the original time value, the  
209 original time value during expiration or inspiration onset and the original time value  
210 during expiration or inspiration offset, respectively. As a result, the expiratory period

The effect of respiration on the brain

211 was scaled into the range [0 1], whereas the inspiratory period was scaled into the  
212 range [1 2] after adding a constant value of one.

213

214 **Phase-coherence analysis.** To detect phase adjustment in brain signals, we  
215 calculated inter-trial phase coherence (ITC), a classical approach that has been  
216 commonly used (Tallon-Baudry et al. 1996). However, to mitigate sample-size bias  
217 while comparing slow- and normal-breathing conditions, we computed the cosine  
218 similarity version of phase coherence ( $ITC_{CS}$ ) to quantify the concentration of phase  
219 clustering across multiple repetitions of the trials locked to the breathing cycle.  $ITC_{CS}$   
220 represents the mean cosine of the angles of all phase pairs from any two trials  $\theta_i, \theta_j$   
221 (Chou and Hsu 2018). This metric produces almost exactly the same pattern of results  
222 as the classical ITC analysis when the sample sizes in two given conditions are similar,  
223 and it approximates the results of bootstrapping at a lower computational cost when  
224 the sample sizes are different. For a given sensor  $s$ , frequency  $f$ , time  $t$ , and a total  
225 number of trials  $N$ ,

$$ITC_{CS}(s, f, t) = \frac{2}{N(N-1)} \sum_{i=1}^{N-1} \sum_{j=i+1}^N \cos(\theta_i - \theta_j).$$

226 An  $ITC_{CS}$  close to 1 reflects strong phase clustering (i.e., all trials exhibit the same  
227 phase). A small or negative  $ITC_{CS}$  reflects low phase coherence, which indicates that  
228 either the distribution of phase angles across trials is uniform or a proportion of the  
229 phase vectors are distant from each other as two diametrically opposed vectors have a  
230 similarity of -1.

231

232 **Source localization.** To localize the significant effects obtained from the sensor-level  
233 phase-coherence analyses, we used a linear constrained minimum variance (LCMV)  
234 algorithm (Bardouille and Ross 2008). We first coregistered the brain surface from  
235 participants' individual segmented MRIs with a single-shell head model. Montreal  
236 Neurological Institute (MNI)-aligned grids were then created in each subject's  
237 individual head space by warping each individual MRI to a template MRI in MNI  
238 coordinates and applying the inverse of this transformation matrix onto the template  
239 dipole grid. With this procedure, a consistent mapping of the spatial positions of grid  
240 points was achieved across participants. For each condition, the covariance matrix  
241 was derived from the bandpass-filtered raw signal using every data point in all the  
242 trials and the information from both the planar gradiometer and the magnetometer  
243 sensors. The lower and upper cut-off frequencies of this time-domain filter were 8 Hz  
244 and 14 Hz (FIR filter) to suppress the noise that was outside the frequency range of  
245 interest (see (Wutz et al. 2014) for a similar procedure). The LCMV beamformer was  
246 then applied to determine the weighting function that estimated the source activity on  
247 the basis of the covariance matrix. Next, we applied the weighting function to the  
248 Hilbert-transformed MEG data within the significant cluster window identified at the  
249 sensor level to calculate phase coherence in source space. This source activity was  
250 then projected onto the individual MNI-aligned grids. Anatomical structures  
251 corresponding to the localized sources were identified using the Automated  
252 Anatomical Labeling (AAL) brain atlas (Tzourio-Mazoyer et al. 2002). Source-level

The effect of respiration on the brain

253 comparisons were calculated using paired t-tests with Benjamini-Hochberg false  
254 discovery rate (FDR) correction.

255

256 **Power analysis.** To compensate for the 1/f decay in power, the choice of the baseline  
257 period for normalization is nontrivial, particularly in the current setting, because all  
258 the data points were task-related and there was no so-called pretrial period for  
259 defining a baseline. Therefore, Z-normalization using the entire trial period as a  
260 baseline was conducted after power was averaged across trials in each experimental  
261 condition for each participant. In the equation

$$P^Z(s, f, t) = \frac{P(s, f, t) - \bar{P}(s, f)}{\sigma(s, f)},$$

262  $P^Z$  denotes the Z-normalized power activity for each sensor  $s$ , frequency  $f$  and time  $t$ ;  
263  $P$  denotes the original activity, and  $\bar{P}$  and  $\sigma$  denote the mean power and the standard  
264 deviation, respectively, of all time points.

265

266 **Cluster-based permutation test.** To determine whether the data differed significantly  
267 between conditions, we conducted cluster-based permutation tests implemented in  
268 FieldTrip. This statistical test does not require specific assumptions about the shape of  
269 the population distribution, and it controls for the problem of multiple comparisons. In  
270 these tests, the conditional differences were quantified by means of paired t-tests for  
271 every sensor-time-frequency sample. The samples with t values exceeding the  
272 threshold ( $p < 0.05$ , two-tailed) were clustered in connected sets based on spatial,  
273 temporal or frequency adjacency. The cluster with the maximum sum of t values was

## The effect of respiration on the brain

274 used as a test statistic. A distribution was then generated by randomly permuting the  
275 data across the conditions for each participant and recalculating the test statistic using  
276 a Monte Carlo estimate after repeating 1000 times. Finally, two-tailed  $p$ -values were  
277 determined by evaluating the proportion of the distribution resulting in a test T  
278 statistic larger than the observed T statistic.

279

280 **Surrogate data.** To confirm that our results were locked to the middle of the  
281 inspiration phase, we surrogated the slow-breathing data by adopting a cut-and-swap  
282 strategy to minimize the distortion of phase dynamics (Aru et al. 2015). Specifically,  
283 during the slow-breathing condition, we randomly selected a single time point and  
284 exchanged the resulting two sections of data in each MEG trial. Next, for every data  
285 point within the significant cluster window, a surrogate  $ITC_{CS}$  was computed and  
286 compared with the initial nonsurrogate  $ITC_{CS}$  during the normal-breathing condition  
287 to generate a new cluster  $t$  statistic (i.e., the sum of  $t$  values within the cluster  
288 window). This procedure was repeated 1000 times, resulting in a distribution of  
289 cluster  $t$ -statistics based on surrogate  $ITC_{CS}$  differences.

290

## 291 **Results**

292 **Slow inspiration reduces cortical phase coherence.** Fifteen participants followed  
293 the centered onscreen cues for when to start inhaling and exhaling and performed  
294 paced breathing at a slow (4 s each for expiration and inspiration or 8 s/breath, i.e.,  
295 0.125 Hz) or normal pace (2 s each for expiration and inspiration or 4 s/breath, i.e.,

## The effect of respiration on the brain

296 0.25 Hz) for a total of 10 min each (Fig. 1a). Consistent with our task instruction,  
297 despite some variability, the breathing rate was  $0.125 \pm < 0.001$  Hz (mean  $\pm$  SD,  
298 collapsed across trials and participants) or  $0.25 \pm < 0.001$  Hz for the slow-breathing or  
299 the normal-breathing condition, respectively. In addition, the duration of the slow or  
300 normal breathing cycle was  $7.83 \pm 0.71$  s or  $3.98 \pm 0.16$  s. Closer examination  
301 revealed that the duration of the expiration phase (slow-breathing:  $4.22 \pm 0.43$  s;  
302 normal-breathing:  $2.09 \pm 0.14$  s) was slightly longer than that of the inspiration phase  
303 (slow-breathing:  $3.61 \pm 0.38$  s; normal-breathing:  $1.89 \pm 0.14$  s) in both conditions.  
304 This observation reflects a common respiratory pattern in which expiration is passive  
305 and requires a longer time for exhalation (Lorig 2007). Despite this, the  
306 inspiration/expiration duration ratios were not significantly different between the two  
307 conditions (two-tailed paired t-test,  $t(14) = 1.30, p = 0.22$ ).

308 To investigate whether cortical phase activity could be modulated by rhythmic  
309 breathing, MEG signals were epoched into trials after aligning them with each  
310 successive pair of peaks of inspiration (Fig. 1a; number of artifact-free trials, slow  
311 breathing:  $52 \pm 9$ ; normal breathing:  $101 \pm 21$ ). Time (the entire epoch)-frequency  
312 (2-14 Hz) representations of the MEG phase data were derived using the filter-Hilbert  
313 transform. Next, inter-trial phase coherence (ITC) was computed to examine the  
314 presence of cortical phase adjustment in response to slow- relative to normal-paced  
315 breathing because this commonly employed measure can quantify to what extent the  
316 phase data at a given sensor-time-frequency point are aligned in the same direction  
317 across the trials that are locked to the repetitions of breathing cycles (i.e., the degree

## The effect of respiration on the brain

318 of event-related phase modulation as a result of repetitive inputs). Given that the  
319 slow- and normal-breathing conditions had different numbers of trials, cosine  
320 similarity was employed instead of the classical ITC analysis to compute phase  
321 coherence in each condition (Chou and Hsu 2018). Unlike ITC, this  $ITC_{CS}$  metric is  
322 robust to sample-size bias, and it computes the mean cosine angle of all phase pairs  
323 from a given trial set (Fig. 1d; see Materials and Methods for details).

324 Although the participants' breathing was paced, the breathing cycles inevitably  
325 contained periodic variation that resulted in variable lengths of respiration-locked  
326 MEG trials within individual participants in each condition (Fig. 1b). This factor may  
327 deteriorate the precision of the phase-coherence computation because the analysis  
328 represents the timing of phase activity across trials. Specifically, if the original time  
329 scale is used, the locus of a given time point for the computation would differ from  
330 trial to trial. In other words, the obtained  $ITC_{CS}$  value at a given time point would  
331 reflect the concentration of phase clustering across multiple repetitions of the trials  
332 locked to different time points along the course of the breathing cycle. To resolve this  
333 issue, for each condition and participant, we conducted unity-based time  
334 normalization by bringing the expiratory time points into the range [0 1] and the  
335 inspiratory time points into the range [1 2] for every trial within individual  
336 participants and conditions (Fig. 1c; see Materials and Methods for details) to  
337 facilitate the subsequent phase-coherence computation and between-condition  
338 comparison. It should be emphasized that the nature of respiration-locked MEG data  
339 or the associated respiratory behavior was not altered because this normalization



## The effect of respiration on the brain

340 procedure simply transformed the varying trial lengths into a common time scale to  
341 consistently describe the course of a breathing cycle such that trials with longer  
342 durations had more MEG data samples to represent a breathing cycle (e.g., trial 1 in  
343 Fig. 1c), whereas trials with shorter durations had fewer data samples (e.g., trial 2 in  
344 Fig. 1c). Because of varying data samples across trials, we used the trial with the  
345 shortest duration as a new time frame because this new frame provides the time  
346 indices that could possibly exist in all the trials. For each of the remaining trials, a  
347 new set of time points was selected based on whether these points were closely  
348 aligned with this time frame (Fig. 1c, red highlights; mean difference between the  
349 selected time points and the time points in the new time frame: slow-breathing  
350 condition = 0.0001 a.u., collapsed across time points, trials and participants;  
351 normal-breathing condition = 0.0002 a.u.). As a result of this data-selection or  
352 “downsampling” procedure, for a given participant and condition, all trials had an  
353 equal number of time points that corresponded to almost equivalent timestamps along  
354 the breathing cycle; thus,  $ITC_{CS}$  that traced the temporal course of breaths could be  
355 properly estimated (slow breathing: number of time points per trial before selection  $\pm$   
356 SD =  $3917 \pm 354$ , collapsed across trials and participants; after selection =  $2782 \pm 626$ ,  
357 collapsed across participants; normal breathing: before selection =  $1991 \pm 82$ ; after  
358 selection =  $1538 \pm 162$ ). After the computation of  $ITC_{CS}$  based on the selected time  
359 points (Fig. 1d), the data-selection procedure was performed again to ensure proper  
360 comparison of group-level  $ITC_{CS}$  between the slow- and normal-breathing conditions  
361 for every sensor-time-frequency MEG data point given that the number of  $ITC_{CS}$

## The effect of respiration on the brain

362 samples along the breathing cycle also varied across the conditions and participants  
363 (Fig. 1e & f, red highlights; mean difference between the selected time points and the  
364 time points in the new time frame: slow-breathing condition = 0.0002 a.u.;  
365 normal-breathing condition = 0.0003 a.u.; number of time points per trial after  
366 selection = 1131).

367 As shown in Fig. 2a, the respiration-locked ITC<sub>CS</sub> values were significantly  
368 reduced during the slow-breathing condition compared with the normal-breathing  
369 condition (cluster-based permutation test to correct for multiple comparison,  $p =$   
370 0.008). The result occurred around the middle of the inspiration period (1.43-1.53 a.u.)  
371 at 8-14 Hz over the left frontal, temporal and occipital magnetometer sensors. Notably,  
372 due to the time-normalization and data-selection procedures, the obtained effect might  
373 initially seem to be transient. When projecting back to the original time scale, this  
374 significant time period actually spanned from approximately 5.54 to 5.92 s (collapsed  
375 across trials and participants) after expiration onset (time = 0 s) in the slow-breathing  
376 condition and from 2.81 to 3.01 s in the normal-breathing condition.

377 To identify the cortical regions that contributed to the effect described here, LCMV  
378 beamforming was performed to recompute ITC<sub>CS</sub> in the source space based on the  
379 significant data points identified at the sensor level. Compared with normal breathing,  
380 a wide range of brain regions consistently reflected reduced ITC<sub>CS</sub> during slow  
381 breathing, ranging from the bilateral occipital and parietal lobes to most of the areas  
382 of the temporal and frontal lobes (Fig. 2b, two-tailed paired t-test with  
383 Benjamini-Hochberg FDR correction,  $t(14) \leq -2.15$ ,  $p < 0.05$ ). A particularly strong

The effect of respiration on the brain

384 reduction (Fig. 2B,  $p < 0.001$ ) was observed in the left superior parietal lobule (MNI  
385 coordinate of peak:  $x = -19$ ,  $y = -80$ ,  $z = 49$ ), left precentral area ( $x = -54$ ,  $y = 0$ ,  $z =$   
386 32) extending to the inferior and middle frontal region, left superior orbital frontal  
387 gyrus ( $x = -18$ ,  $y = 39$ ,  $z = -20$ ), right middle frontal gyrus ( $x = 50$ ,  $y = 20$ ,  $z = 40$ ) and  
388 right inferior temporal gyrus ( $x = 50$ ,  $y = -31$ ,  $z = -25$ ).

389

390 **Reduced phase coherence could not be attributed to the potential caveats of the**

391 **analyses.** Our analysis approach might have biased the results. In particular, the trial  
392 lengths differed significantly between the slow- and normal-breathing conditions;  
393 therefore, the  $ITC_{CS}$  values in the slow-breathing condition were “downsampled” to  
394 some extent during the group-level data-selection step (Fig. 1f). To assess the impact  
395 of this process on estimating  $ITC_{CS}$  in the slow-breathing condition, we calculated and  
396 averaged the original  $ITC_{CS}$  values, which refer to the values obtained before  
397 group-level data selection within the significant cluster window. These original data  
398 from the slow-breathing condition were then contrasted with the initial data from the  
399 normal-breathing condition, which refer to the values obtained after group-level data  
400 selection and within the significant window. Still, reduced phase coherence was  
401 obtained (two-tailed paired t-test,  $t(14) = -7.49$ ,  $p < 0.001$ ).

402 To additionally ensure that the group-level data-selection step did not happen to  
403 select the data points with extreme values and, in turn, lead to a significant result, a  
404 resampling procedure was applied for the slow-breathing condition. In this procedure,  
405 each participant’s original  $ITC_{CS}$  values (i.e., before group-level data selection) in the

## The effect of respiration on the brain

406 significant cluster window were randomly selected without replacement to match the  
407 number of data points that were initially obtained (i.e., after group-level data  
408 selection). Next, we computed the mean for these samples. This procedure was  
409 repeated 1,000 times to generate a resampling distribution of  $ITC_{CS}$  that was derived  
410 from the initial sample size and represented the resampled means in the cluster  
411 window during slow breathing. For every participant, the initially obtained  $ITC_{CS}$   
412 mean fell within the 95% confidence interval of the distribution (location: mean  $\pm$  SD  
413 = 40.33%  $\pm$  13.32, range = 22.3 - 67.2%, above the lower bound), indicating that the  
414 group-level data-selection process did not substantially distort the results.

415 Because of the slight variability of the trial length in each condition, trial-level data  
416 selection should have little impact on the result (Fig. 1c). Nevertheless, a similar  
417 resampling procedure was conducted to ensure its validity. For this analysis, the  
418 original phases (i.e., before trial-level data selection) within the significant cluster  
419 window were resampled and averaged to generate a resampling distribution of the  
420 mean phase. For every participant, the initially obtained phase mean (i.e., after  
421 trial-level data selection) also fell within the confidence interval of the distribution  
422 (slow breathing: mean  $\pm$  SD = 49.17%  $\pm$  6.50, range = 40.83 - 60.32%, collapsed  
423 across trials; normal breathing: 48.43%  $\pm$  4.74, 40.34 - 60.44%).

424

425 **Reduced phase coherence is specifically locked to ongoing inspiration.** To verify  
426 that reduced  $ITC_{CS}$  values were genuinely time locked to the middle of the inspiration  
427 phase, we shuffled the phase data from the slow-breathing condition to create

The effect of respiration on the brain

428 surrogate  $ITC_{CS}$  while the initial phase data from the normal-breathing condition  
429 remained untouched. Because  $ITC_{CS}$  represents the timing of phase activity over trials,  
430 the null hypothesis is that shifting the phase time series during the slow-breathing  
431 condition by a random amount (i.e., not locked to inspiration) would not affect its  
432  $ITC_{CS}$  strength relative to that during the normal-breathing condition. For each MEG  
433 trial, we randomly selected a single time point of the phase data (Fig. 1b) and  
434 exchanged the resulting two sections of data so that the original phase information  
435 was retained with minimal distortion. After the  $ITC_{CS}$  computation, we recomputed  
436 the cluster t-statistics by contrasting surrogate  $ITC_{CS}$  from the slow-breathing  
437 condition with initial  $ITC_{CS}$  from the normal-breathing condition for individual data  
438 points within the significant cluster window. The entire analysis procedure was  
439 repeated 1000 times (Fig. 1b to 1f) such that a distribution of cluster t-statistics under  
440 the null hypothesis was generated. The initially obtained statistics were found to  
441 exceed all the surrogate ones (i.e.,  $p < 0.001$ ), thereby confirming that the observed  
442 effects were significantly locked to ongoing inspiration.

443

444 **Reduced phase coherence is not accompanied by respiration-locked power, ERF**  
445 **or cardiac activity effects.** Differences in the amplitude of event-related  
446 potentials/fields (ERPs/ERFs) or power may produce differing phase-coherence  
447 values that are independent of any actual change in the phase (van Diepen and  
448 Mazaheri 2018). Through a similar analysis pipeline including time normalization,  
449 trial-level and group-level data selection, raw MEG and single-trial normalized power

## The effect of respiration on the brain

450 activities were computed for each condition and participant, respectively. No  
451 significant difference in power (Fig. 3a, cluster-based permutation test,  $p = 0.57$ ) or  
452 ERF amplitude (Fig. 3b,  $p = 1$ ) was found between the slow- and normal-breathing  
453 conditions. The same results were obtained even when the analyses were restricted in  
454 the reported sensor-time-frequency (two-tailed paired t-test on the mean data within  
455 the significant cluster window,  $t(14) = -0.70$ ,  $p = 0.50$ ) or sensor-time window ( $t(14) =$   
456  $1.11$ ,  $p = 0.29$ ). The absence of a respiration-locked power difference further  
457 undermines the possibility that our results reflect a discrepancy in phase estimation  
458 due to differential power or that the results could be ascribed to differential task  
459 demands, as indexed by widespread alpha power differentiation (Fink et al. 2005;  
460 Jensen et al. 2002; Mahjoory et al. 2019).

461 The cardiovascular and respiratory systems strongly interact (Angelone and Coulter  
462 1964). Therefore, cardiovascular input might contribute an indirect effect. We  
463 investigated whether there was a difference in cardiac activity between the two  
464 conditions and whether such a change could characterize the observed results. To  
465 account for variation in trial lengths across participants and conditions, we discretized  
466 each trial into 16 time bins with 8 bins each during inspiration and expiration, where  
467 bin 12 approximately corresponded to the timing of the reported phase-coherence  
468 result. Next, we counted the occurrence of QRS complexes within each time bin in  
469 simultaneously recorded ECG. The obtained results were expressed as the number of  
470 QRS complexes per second and averaged over trials for individual participants (Fig.  
471 3c). Consistent with so-called respiratory sinus arrhythmia (Angelone and Coulter

## The effect of respiration on the brain

1964) and previous reports that slow breathing is associated with increasing heart-rate fluctuation (Lehrer and Gevirtz 2014; Radaelli et al. 2004), QRS frequency significantly accelerated during ongoing inspiration and slowed during ongoing expiration in the slow-breathing condition (one-way repeated-measure ANOVA,  $F(15,180) = 4.68, p < 0.001$ ) but not in the normal-breathing condition ( $F(15,180) = 1.28, p = 0.22$ ). Despite the results, the time courses of QRS frequency were not significantly different between the two conditions (two-way repeated-measures ANOVA on interaction,  $F(15,180) = 0.74, p = 0.74$ ), indicating that the patterns of the QRS complex could not fully characterize our findings.

481

**Reduced phase coherence reflects increasing phase distance between the respiration-locked trials in the slow-breathing condition.** Reduced phase coherence indices commonly indicate that phase angles are becoming randomly distributed across trials. However,  $ITC_{CS}$  may also decrease if large phase differences exist in some subsets of trial pairs because similarity measurements become more negative when the cosine of the angle between the two phases in these pairs becomes diametrically opposed (see Fig. 4 for details). To investigate the nature of the phase dynamics underlying our results, we examined the distribution of absolute phase differences in the significant sensor-time-frequency points. On the one hand, this examination reflects the intrinsic process during  $ITC_{CS}$  computation. On the other hand, because the exact pattern of the phase distribution at each data point differed greatly (Supplementary Fig. S1 (<https://doi.org/10.5281/zenodo.3466135>)), the

## The effect of respiration on the brain

494 distribution of absolute phase differences (i.e., phase distance in each pair of phase  
495 samples), which represents the phase composition in a relative fashion, was more  
496 suitable than the phase distribution per se for detecting the converging pattern  
497 revealed from the overall data within the significant cluster window (Supplementary  
498 Fig. S2 (<https://doi.org/10.5281/zenodo.3466135>)).

499 For every significant sensor-time-frequency point, the absolute phase differences  
500 between every two trials in all possible combinations were first calculated. In other  
501 words, for this analysis, we followed the same  $ITC_{CS}$  computation (Fig. 1d) except  
502 that the phase differences were not averaged but their absolute values were grouped  
503 together. The results were then pooled together across all the data points for each  
504 participant and condition. The final results were discretized into 20 bins according to  
505 the phase difference, and in each bin, the relative probability of occurrence was  
506 calculated. As shown in Fig. 5, slow breathing regularized the distribution of phase  
507 differences in a consistent and specific manner. For every individual participant, there  
508 was an increasing number of trial pairs whose phases were moving from each other  
509 during the slow-breathing condition (t-test on the slope of the regression line, sub1:  
510  $t(18) = 9.80, p < 0.001$ , sub2:  $t(18) = 9.58, p < 0.001$ ; see Supplementary Fig. S3  
511 (<https://doi.org/10.5281/zenodo.3466135>) for the results from the rest of the  
512 participants:  $ts \geq 5.34, ps < 0.001$ ). However, during the normal-breathing condition,  
513 the opposite pattern was found in 8 out of 15 participants (Fig. 5b, sub1:  $t(18) =$   
514  $-16.88, p < 0.001$ ; Fig. S3,  $ts \leq -2.84, ps \leq 0.05$ ), while one followed the pattern  
515 generally observed in the slow-breathing condition (Fig. S3,  $t(18) = 4.42, p < 0.001$ ).



## The effect of respiration on the brain

516 For the remaining 6 participants, the distribution did not significantly change  
517 according to the phase difference (Fig. 5b, sub2:  $t(18) = -1.50$ ,  $p = 0.15$ ; Fig. S3,  $-1.5$   
518  $\geq ts \geq -1.76$ ,  $0.15 \geq ps \geq 0.10$ ). Thus, for most of the participants, the  
519 normal-breathing phases were either clustered around a similar direction or randomly  
520 distributed and approaching uniform.

521

## 522 **Discussion**

523 The current study shows that cortical alpha phase activity can be modulated by  
524 rhythmic inputs from controlled slow breathing. The findings extend and advance our  
525 understanding of several aspects of the interaction between the respiratory system and  
526 the brain. First, during ongoing slow breathing relative to normal breathing, phase  
527 coherence was reduced over a wide range of brain areas, spanning most of the area of  
528 the temporal and prefrontal lobes. This finding is consistent with prior animal and  
529 human evidence that these two lobes are involved in respiration-entrained neural  
530 activity (Herrero et al. 2018; Tort et al. 2018) and indicates that slow breathing could  
531 affect phase dynamics in a large part of the brain. However, our results appear to be  
532 locked to ongoing inspiration as opposed to expiration. This observation could be a  
533 consequence of different mechanistic or evolutionary mechanisms involved in these  
534 two stages of breathing. In contrast to inspiration, expiration is largely passive and  
535 reflects the result of relaxation of the external intercostals and diaphragm (Lorig  
536 2007), whereas inspiration is an active process and prepares the brain to receive  
537 incoming sensory information (Corcoran et al. 2018). These two respiratory stages

## The effect of respiration on the brain

538 might be differentially translated in the brain, irrespective of the underlying  
539 mechanism. Indeed, compared with expiration, ongoing inspiration is associated with  
540 pain perception (Arsenault et al. 2013), near-threshold stimuli detection (Flexman et  
541 al. 1974), fearful expression discrimination (Zelano et al. 2016), and visuospatial  
542 performance (Perl et al. 2019). Our finding thus provides a novel complement to the  
543 existing data and emphasizes the unique role of inspiration in cortical phase activity  
544 and potentially in accompanying cognitive functions.

545 Our further analyses go beyond the finding of reduced phase coherence and identify  
546 how slow breathing adjusts the pattern of phase dynamics that orchestrates the  
547 mechanism underlying the finding (see Supplementary Fig. S4  
548 (<https://doi.org/10.5281/zenodo.3466135>) for the argument of noncircular inference).  
549 At the single-subject level, slow inspiration systematically organized the phase  
550 distribution such that phases became more likely to be diametrically opposed across  
551 the trials. In contrast, the phase distribution driven by normal inspiration tended to be  
552 unsettled, either clustering around a single direction or becoming randomized. Thus,  
553 the inherently coherent phase structure indicates the presence of consistent phase  
554 adjustment in response to slow-paced inspiratory inputs. Accordingly, the present  
555 results not only support our hypothesis that breathing dynamically shapes cortical  
556 phase activity but also imply that slow inspiration organizes the cortical phase in a  
557 rather regularized pattern. By virtue of this mechanism, we propose, rather  
558 speculatively, that the coding of existing or subsequent inputs could be suppressed  
559 during slow breathing because phase-mediated neural transmission or communication

## The effect of respiration on the brain

560 might be either disrupted for preceding inputs or less susceptible to readjustment for  
561 subsequent inputs due to the regularized phase pattern imposed by slow inspiration.  
562 This idea echoes other phase-adjustment phenomena during extrinsic stimulation in  
563 which, during attention selection, for example, the oscillatory phase adjusted by  
564 attended stimuli prevents the coding of unattended stimuli (Schroeder and Lakatos  
565 2009; Voloh and Womelsdorf 2016). Distinctively, we suggest that cortical phase  
566 adjustment can be internally governed based on volitional control of rhythmic inputs  
567 from a bodily source, namely, respiration, and not merely from extrinsic stimulation.

568 Our study also reveals a unique pattern of phase adjustment that has seldom been  
569 described. In contrast to prior reports, the adjusted phase does not cluster toward a  
570 certain direction; instead, the phase is adjusted in such a manner that the phase angles  
571 tend to be distant from each other across trials, resulting in reduced phase coherence.  
572 This finding highlights a shortcoming in commonly adopted phase-coherence analysis  
573 in which a high value is usually construed as reflecting consistent phase adjustment.  
574 Here, we show that phase adjustment does not necessarily accompany a high  
575 phase-coherence value if the shape of the phase distribution is not unimodal (Fig. 4).  
576 Alternatively, examining the distribution of absolute phase differences, as  
577 demonstrated in the current approach, might provide a window to gain better insights  
578 into the nature of phase coherence.

579 Although participants' breaths were paced throughout the study, different  
580 task-related effects might exist between the slow- and normal-breathing conditions  
581 that are not relevant to breathing per se. However, our results are unlikely to reflect

## The effect of respiration on the brain

582 differential task demands because of a lack of widespread, task-dependent alpha  
583 power modulation between the conditions (Fink et al. 2005; Jensen et al. 2002;  
584 Mahjoory et al. 2019). Additionally, the participants did not seem to exhibit a notably  
585 increased degree of awareness of slow breaths compared with normal breaths as  
586 strong activation of interoception-related neural correlates – such as the anterior  
587 cingulate cortex and the insula (Herrero et al. 2018) – should be expected. Above all,  
588 these interpretations are not easily reconcilable with the specific role of ongoing  
589 inspiration in our results, and the latter interpretations are often associated with  
590 enhanced phase-coherence values (Park et al. 2018), which contradicts the present  
591 results. Nevertheless, partly due to technical constraints, cardiorespiratory parameters,  
592 such as blood pressure and diaphragmatic breathing, were not measured exhaustively.  
593 Thus, the effects of these additional parameters on the present findings remain to be  
594 determined. Moreover, future research needs to clarify whether the effect of slow  
595 breathing could be present during natural breathing when there is a lack of volitional  
596 control of breathing.

597     Respiration-entrained neural oscillations are thought to act as an integral part of  
598 rhythmic brain activity (Heck et al. 2017; Tort et al. 2018). Akin to this idea, by  
599 applying periodic perturbation through different breathing paces, the current study  
600 demonstrates that cortical phase dynamics can be systematically altered in response to  
601 such perturbation. This finding implies that the respiration-locked phase effects  
602 constitute a fundamental organizing principle of brain activity, thus uncovering a  
603 complex rhythmic neural network integrated with different neurophysiological

The effect of respiration on the brain

604 systems. It is interesting to note that slow breathing is associated with cognitive and  
605 emotional changes (Boiten et al. 1994; Homma and Masaoka 2008; Kreibig 2010).  
606 The overall results may shed light on how a volitionally controlled change in  
607 respiratory behavior will perturb the rhythmic brain-respiration network and  
608 ultimately regulate cognitive and emotional behavior.

609

## 610 **Acknowledgments**

611 This work was supported by the Ministry of Science and Technology, R.O.C.  
612 (MOST 108-2634-F-002-022, MOST 107-2420-H-002-031-RE2 and  
613 MOST104-2420-H-002-016-MY3-L10605). The authors thank Jun-Wei Huang for  
614 assistance in data preprocessing and Li Yu, José Luis and Michael Rosenblum for  
615 commenting on an early version of the manuscript.

616

## 617 **References**

- 618 **Angelone A, and Coulter NA.** Respiratory sinus arrhythmia: a frequency dependent  
619 phenomenon. *J Appl Physiol* 19: 479-482, 1964.
- 620 **Arsenault M, Ladouceur A, Lehmann A, Rainville P, and Piche M.** Pain  
621 modulation induced by respiration: phase and frequency effects. *Neuroscience* 252:  
622 501-511, 2013.
- 623 **Aru J, Aru J, Priesemann V, Wibral M, Lana L, Pipa G, Singer W, and Vicente R.**  
624 Untangling cross-frequency coupling in neuroscience. *Curr Opin Neurobiol* 31: 51-61,  
625 2015.
- 626 **Bardouille T, and Ross B.** MEG imaging of sensorimotor areas using inter-trial

The effect of respiration on the brain

- 627 coherence in vibrotactile steady-state responses. *Neuroimage* 42: 323-331, 2008.
- 628 **Barrett KE, Barman SM, Boitano S, and Brooks H.** Ganong's review of medical  
629 physiology. New York: McGraw-Hill Medical, 2010.
- 630 **Boiten FA, Frijda NH, and Wientjes CJE.** Emotions and respiratory patterns -  
631 review and critical analysis. *Int J Psychophysiol* 17: 103-128, 1994.
- 632 **Chou EP, and Hsu SM.** Cosine similarity as a sample size-free measure to quantify  
633 phase clustering within a single neurophysiological signal. *J Neurosci Meth* 295:  
634 111-120, 2018.
- 635 **Corcoran AW, Pezzulo G, and Hohwy J.** Commentary: Respiration-entrained brain  
636 rhythms are global but often overlooked. *Front Syst Neurosci* 12: 2018.
- 637 **Critchley HD, and Garfinkel SN.** The influence of physiological signals on  
638 cognition. *Curr Opin Behav Sci* 19: 13-18, 2018.
- 639 **Del Negro CA, Funk GD, and Feldman JL.** Breathing matters. *Nat Rev Neurosci* 19:  
640 351-367, 2018.
- 641 **Fink A, Grabner RH, Neuper C, and Neubauer AC.** EEG alpha band dissociation  
642 with increasing task demands. *Cognitive Brain Res* 24: 252-259, 2005.
- 643 **Flexman JE, Demaree RG, and Simpson DD.** Respiratory phase and visual  
644 signal-detection. *Percept Psychophys* 16: 337-339, 1974.
- 645 **Heck DH, McAfee SS, Liu Y, Babajani-Feremi A, Rezaie R, Freeman WJ,**  
646 **Wheless JW, Papanicolaou AC, Ruzinko M, and Kozma R.** Breathing as a  
647 fundamental rhythm of brain function. *Front Neural Circuit* 10: 1-8, 2017.
- 648 **Herrero JL, Khuvis S, Yeagle E, Cerf M, and Mehta AD.** Breathing above the

The effect of respiration on the brain

- 649 brain stem: volitional control and attentional modulation in humans. *J Neurophysiol*  
650 119: 145-159, 2018.
- 651 **Homma I, and Masaoka Y.** Breathing rhythms and emotions. *Exp Physiol* 93:  
652 1011-1021, 2008.
- 653 **Ito J, Roy S, Liu Y, Cao Y, Fletcher M, Lu L, Boughter JD, Grun S, and Heck**  
654 **DH.** Whisker barrel cortex delta oscillations and gamma power in the awake mouse  
655 are linked to respiration. *Nat Commun* 5: 1-10, 2014.
- 656 **Jensen O, Gelfand J, Kounios J, and Lisman JE.** Oscillations in the alpha band  
657 (9-12 Hz) increase with memory load during retention in a short-term memory task.  
658 *Cereb Cortex* 12: 877-882, 2002.
- 659 **Kreibig SD.** Autonomic nervous system activity in emotion: A review. *Biol Psychol*  
660 84: 394-421, 2010.
- 661 **Lakatos P, Karmos G, Mehta AD, Ulbert I, and Schroeder CE.** Entrainment of  
662 neuronal oscillations as a mechanism of attentional selection. *Science* 320: 110-113,  
663 2008.
- 664 **Lehrer PM, and Gevirtz R.** Heart rate variability biofeedback: how and why does it  
665 work? *Front Psychol* 5: 2014.
- 666 **Lorig TS.** The respiratory system. In: *Handbook of psychophysiology*, edited by  
667 Cacioppo JT, Tassinary LG, and Berntson GG. Cambridge England ; New York:  
668 Cambridge University Press, 2007, p. 231-243.
- 669 **Luo H, and Poeppel D.** Phase patterns of neuronal responses reliably discriminate  
670 speech in human auditory cortex. *Neuron* 54: 1001-1010, 2007.

The effect of respiration on the brain

- 671 **Lutz A, Greischar LL, Rawlings NB, Ricard M, and Davidson RJ.** Long-term  
672 meditators self-induce high-amplitude gamma synchrony during mental practice. *P*  
673 *Natl Acad Sci USA* 101: 16369-16373, 2004.
- 674 **Mahjoory K, Cesnaite E, Hohlefeld FU, Villringer A, and Nikulin VV.** Power and  
675 temporal dynamics of alpha oscillations at rest differentiate cognitive performance  
676 involving sustained and phasic cognitive control. *Neuroimage* 188: 135-144, 2019.
- 677 **Oostenveld R, Fries P, Maris E, and Schoffelen JM.** FieldTrip: Open source  
678 software for advanced analysis of MEG, EEG, and invasive electrophysiological data.  
679 *Computational Intelligence and Neuroscience* 2011: 156869, 2011.
- 680 **Pan J, and Tompkins WJ.** A real-time QRS detection algorithm. *Ieee T Bio-Med Eng*  
681 32: 230-236, 1985.
- 682 **Park HD, Bernasconi F, Salomon R, Tallon-Baudry C, Spinelli L, Seeck M,**  
683 **Schaller K, and Blanke O.** Neural sources and underlying mechanisms of neural  
684 responses to heartbeats, and their role in bodily self-consciousness: An intracranial  
685 EEG study. *Cereb Cortex* 28: 2351-2364, 2018.
- 686 **Paul NA, Stanton SJ, Greeson JM, Smoski MJ, and Wang LH.** Psychological and  
687 neural mechanisms of trait mindfulness in reducing depression vulnerability. *Soc*  
688 *Cogn Affect Neur* 8: 56-64, 2013.
- 689 **Perl O, Ravia A, Rubinson M, Eisen A, Soroka T, Mor N, Secundo L, and Sobel**  
690 **N.** Human non-olfactory cognition phase-locked with inhalation. *Nat Hum Behav* 3:  
691 501-512, 2019.
- 692 **Radaelli A, Raco R, Perfetti P, Viola A, Azzellino A, Signorini MG, and Ferrari**



The effect of respiration on the brain

- 693 **AU.** Effects of slow, controlled breathing on baroreceptor control of heart rate and  
694 blood pressure in healthy men. *J Hypertens* 22: 1361-1370, 2004.
- 695 **Sauseng P, and Klimesch W.** What does phase information of oscillatory brain  
696 activity tell us about cognitive processes? *Neurosci Biobehav R* 32: 1001-1013, 2008.
- 697 **Spaak E, de Lange FP, and Jensen O.** Local entrainment of alpha oscillations by  
698 visual stimuli causes cyclic modulation of perception. *J Neurosci* 34: 3536-3544,  
699 2014.
- 700 **Stefanics G, Hangya B, Hernadi I, Winkler I, Lakatos P, and Ulbert I.** Phase  
701 entrainment of human delta oscillations can mediate the effects of expectation on  
702 reaction speed. *J Neurosci* 30: 13578-13585, 2010.
- 703 **Tallon-Baudry C, Bertrand O, Delpuech C, and Pernier J.** Stimulus specificity of  
704 phase-locked and non-phase-locked 40 Hz visual responses in human. *J Neurosci* 16:  
705 4240-4249, 1996.
- 706 **Thut G, Miniussi C, and Gross J.** The functional importance of rhythmic activity in  
707 the brain. *Curr Biol* 22: R658-R663, 2012.
- 708 **Tort ABL, Brankack J, and Draguhn A.** Respiration-entrained brain rhythms are  
709 global but often overlooked. *Trends Neurosci* 41: 186-197, 2018.
- 710 **Tzourio-Mazoyer N, Landeau B, Papathanassiou D, Crivello F, Etard O,**  
711 **Delcroix N, Mazoyer B, and Joliot M.** Automated anatomical labeling of activations  
712 in SPM using a macroscopic anatomical parcellation of the MNI MRI single-subject  
713 brain. *Neuroimage* 15: 273-289, 2002.
- 714 **van Diepen RM, and Mazaheri A.** The caveats of observing inter-trial

The effect of respiration on the brain

- 715 phase-coherence in cognitive neuroscience. *Sci Rep-Uk* 8: 1-9, 2018.
- 716 **vanRullen R.** Perceptual Cycles. *Trends Cogn Sci* 20: 723-735, 2016.
- 717 **Varela F, Lachaux JP, Rodriguez E, and Martinerie J.** The brainweb: Phase  
718 synchronization and large-scale integration. *Nat Rev Neurosci* 2: 229-239, 2001.
- 719 **Varga S, and Heck DH.** Rhythms of the body, rhythms of the brain: Respiration,  
720 neural oscillations, and embodied cognition. *Conscious Cogn* 56: 77-90, 2017.
- 721 **Voloh B, and Womelsdorf T.** A role of phase-resetting in coordinating large scale  
722 neural networks during attention and goal-directed behavior. *Front Syst Neurosci* 10:  
723 2016.
- 724 **Wutz A, Weisz N, Braun C, and Melcher D.** Temporal windows in visual processing:  
725 "prestimulus brain state" and "poststimulus phase reset" segregate visual transients on  
726 different temporal scales. *J Neurosci* 34: 1554-1565, 2014.
- 727 **Zeidan F, Johnson SK, Diamond BJ, David Z, and Goolkasian P.** Mindfulness  
728 meditation improves cognition: Evidence of brief mental training. *Conscious Cogn* 19:  
729 597-605, 2010.
- 730 **Zelano C, Jiang HD, Zhou GY, Arora N, Schuele S, Rosenow J, and Gottfried JA.**  
731 Nasal respiration entrains human limbic oscillations and modulates cognitive function.  
732 *J Neurosci* 36: 12448-12467, 2016.

733

### 734 **Figure captions**

735 **Figure 1. Schematic illustration of the analysis pipeline. (a)** Participants performed  
736 paced breathing by following the cues “|” and “ - ” at the center of the screen, which

## The effect of respiration on the brain

737 indicated the onset of expiration and inspiration. The alternation rate between the two  
738 cues was either 2 s (normal breathing) or 4 s (slow breathing), resulting in 4 s/ breath  
739 in the normal-breathing condition and 8 s/ breath in the slow-breathing condition. The  
740 recorded MEG data at a given sensor were epoched into trials aligned to each  
741 successive pair of peaks of inspiration (corresponding to one breath) and extended  
742 from 1 s before to 1 s after the peaks to avoid edge effects during spectral analysis. **(b)**  
743 For each trial, the respiration-locked MEG phase data were computed using the  
744 Hilbert transform after bandpass filtering the data to create 13 frequency steps  
745 between 2 and 14 Hz. Note that the sensor and frequency dimensions are not  
746 illustrated here. **(c)** Because of slightly variable MEG trial lengths within each  
747 participant and condition, the expiration- and inspiration-locked periods of each trial  
748 were normalized to the time ranges [0 1] and [1 2]. The dots represent individual  
749 normalized time points. For a given participant and condition, a new set of MEG time  
750 points in each trial was selected based on the time frame from the trial with the  
751 shortest duration (red highlight). **(d)** Phase coherence across respiration-locked trials  
752 ( $ITC_{CS}$ ) was derived by computing the mean cosine angle of all phase pairs from two  
753 given trials at each selected data point. **(e, f)** Because of variable  $ITC_{CS}$  time points  
754 between participants and conditions, the same data-selection procedure was  
755 performed on the time domain for the group-level analysis using the time frame from  
756 the participant/condition with the shortest duration (red highlight). RESP, respiration;  
757 EX, expiration; IN, inspiration; S.B., slow breathing; N.B., normal breathing.  
758

## The effect of respiration on the brain

759 **Figure 2. Reduced phase coherence during slow breathing relative to normal**  
760 **breathing. (a)** The left scalp topography expresses the  $t$  statistic (slow breathing vs.  
761 normal breathing) of the cluster of significant sensors (red dot; cluster-based  
762 permutation,  $p = 0.008$ ) at peak 10 Hz and time 1.48 (a.u.). The middle panel  
763 expresses the time-frequency representation of the  $t$  statistic averaged from the  
764 significant sensors. The red brackets (8-14 Hz) highlight the frequency range of the  
765 cluster. The right panel shows the time course of averaged raw  $ITC_{CS}$  values from the  
766 significant sensor-frequency points. The red horizontal bar highlights the significant  
767 time period of the cluster. Notably, the expiratory/inspiratory time scales were  
768 normalized to the ranges [0 1]/[1 2]. In the original time scale, the significant time  
769 period corresponded to approximately 5.54-5.92 s (collapsed across trials and  
770 participants) after expiration onset (time = 0 s) in the slow-breathing condition and  
771 2.81-3.01 s in the normal-breathing condition. Shaded regions indicate 95%  
772 confidence intervals. S.B., slow breathing; N.B., normal breathing; a.u., arbitrary  
773 unit. **(b)** The sources of reduced  $ITC_{CS}$  during slow relative to normal breathing, as  
774 localized by the LCMV beamformer, are located over the bilateral occipital, temporal,  
775 and parietal to frontal lobes (two-tailed paired  $t$ -test with FDR correction,  $p < 0.05$ ;  $t$   
776 values below an  $\alpha$ -level of 0.05 are masked) and are prominent in the left superior  
777 parietal lobule, left precentral gyrus, left superior orbital frontal gyrus, right middle  
778 frontal gyrus and right inferior temporal gyrus (red circle;  $p < 0.001$ ). To improve  
779 visualization of the left superior orbital frontal gyrus (right panel) and right inferior

The effect of respiration on the brain

780 temporal gyrus (left panel), the sagittal views are also illustrated (solid red circle;  $t$   
781 values below an  $\alpha$ -level of 0.001 are masked).

782

783 **Figure 3. No significant difference in respiration-locked power ERF or cardiac**

784 **activity during slow breathing relative to normal breathing. (a) The scalp**

785 **topography expresses the  $t$  statistic (slow breathing vs. normal breathing) at 10 Hz**

786 **and time 1.48 (a.u.). The middle panel expresses the time-frequency representation of**

787 **the  $t$  statistic averaged from the sensors highlighted in white, i.e., previously reported**

788 **significant sensors. The right panel shows the time courses of averaged 8-14 Hz**

789 **power from the highlighted sensors. The expiratory/inspiratory period was**

790 **normalized to the ranges [0 1]/[1 2]. (b) The scalp topography expresses the  $t$  statistic**

791 **(slow breathing vs. normal breathing) at time 1.48 (a.u.). The right panel shows the**

792 **time courses of averaged ERFs from the highlighted sensors. (c) The time courses of**

793 **the frequency of the QRS complex are illustrated. The expiratory/inspiratory period**

794 **was binned into the ranges [1 8]/[9 16]. All shaded regions indicate 95% confidence**

795 **intervals. S.B., slow breathing; N.B., normal breathing; a.u., arbitrary unit.**

796

797 **Figure 4. Relations among  $ITC_{CS}$ , phase distribution, and distribution of absolute**

798 **phase difference as illustrated using simulated phase data. Data were generated by**

799 **randomly selecting 50 phase samples from  $-\pi/4$  to  $\pi/4$  (left panel),  $-\pi$  to  $\pi$  (middle**

800 **panel) or a mixture of 10 phases from 0 to  $\pi$  and 20 sample pairs with half of the**

801 **samples from 0 to  $\pi$  and the other half at the opposite angles (right panel). This data**

802 **generation procedure was repeated 1000 times. The top panel shows  $ITC_{CS}$  averaged**

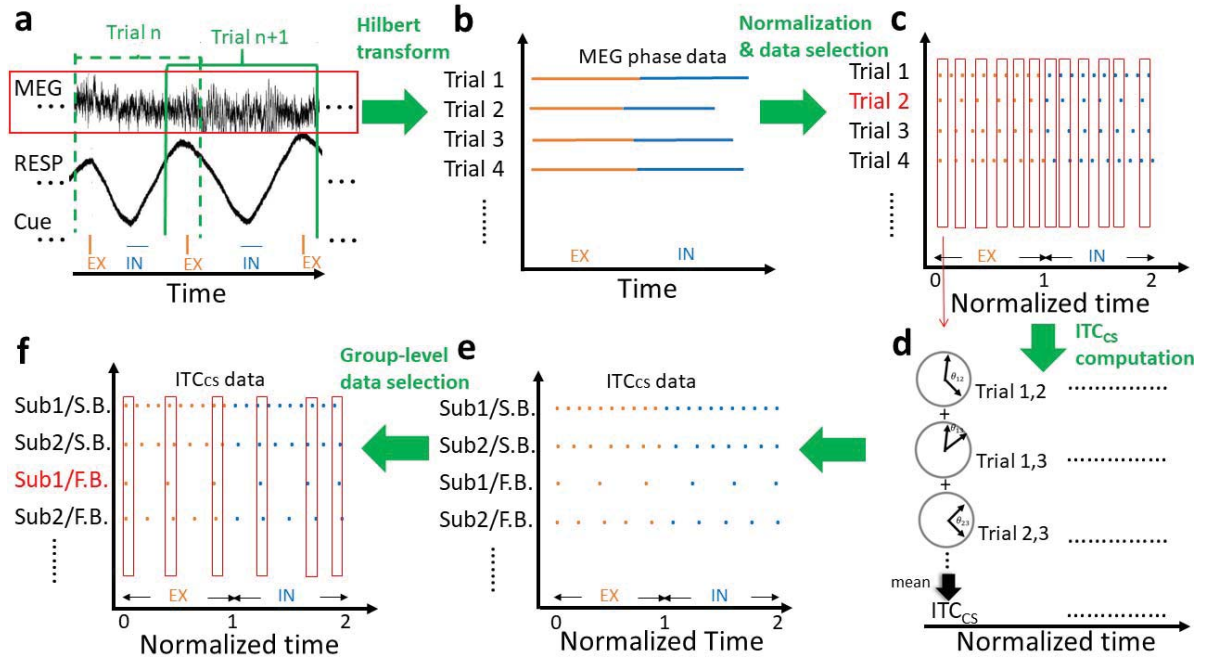
The effect of respiration on the brain

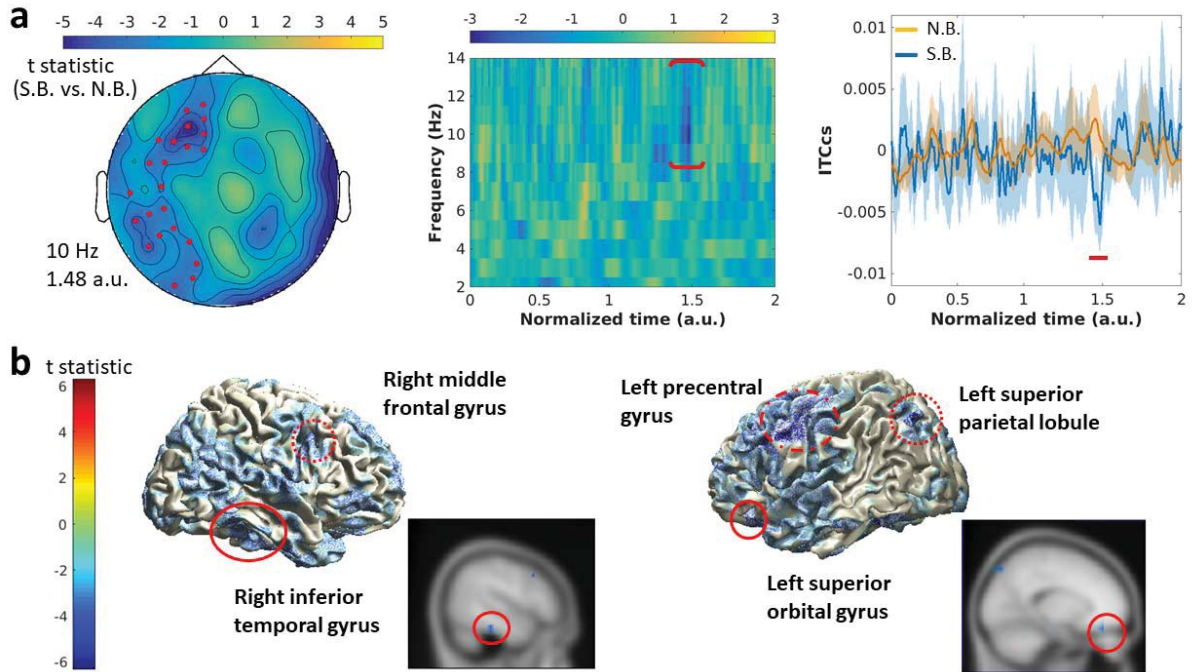
803 *across repetitions. The circular and horizontal histograms depict the phase*  
804 *distributions and the distributions of absolute phase differences (i.e., phase distance*  
805 *between every two possible phase samples in a given data set) collapsed across*  
806 *samples from all repetitions.*

807

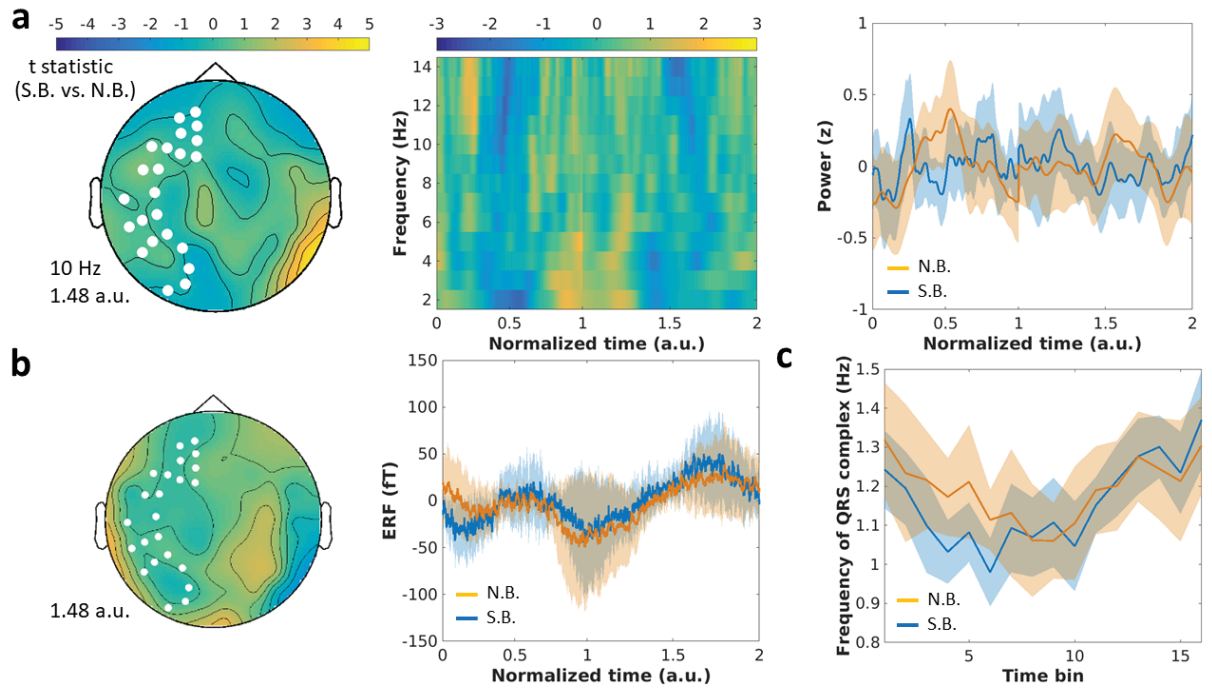
808 ***Figure 5. Distinct phase patterns driven by slow and normal breathing as revealed***  
809 ***from the distribution of absolute phase differences. The horizontal histograms depict***  
810 ***the distributions of absolute phase differences collapsed across all significant data***  
811 ***points from two representative participants during the slow- (top panel) and***  
812 ***normal-breathing (bottom panel) conditions. Red lines represent the linear regression***  
813 ***lines. \*\*\* $p < 0.001$ .***

814

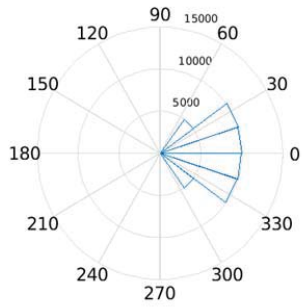




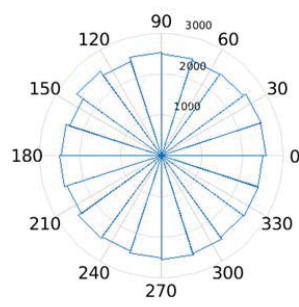




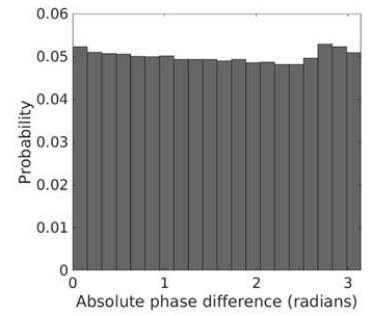
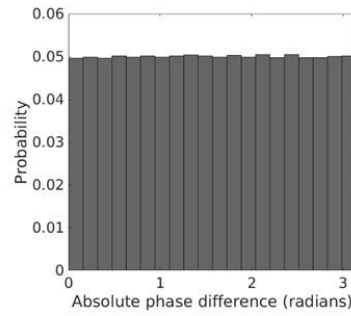
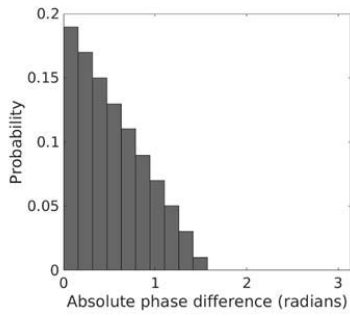
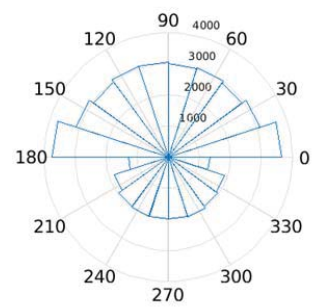
$ITC_{CS} = 0.810$



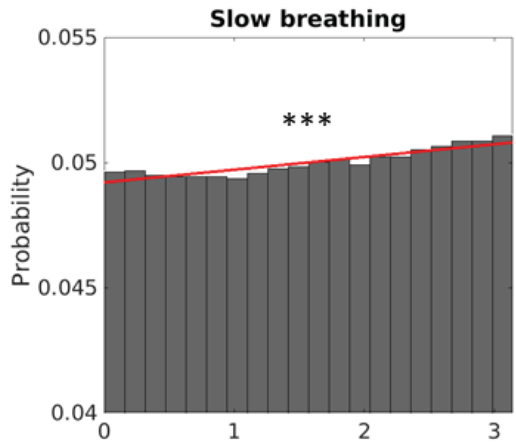
$ITC_{CS} = 0$



$ITC_{CS} = 0.003$



### Sub 1



### Sub 2

